nature communications

Article

https://doi.org/10.1038/s41467-024-52851-z

Nanomaterial inactivates environmental virus and enhances plant immunity for controlling tobacco mosaic virus disease

Received: 10 July 2024

Accepted: 23 September 2024

Published online: 01 October 2024

Check for updates

Qinhong Jiang[1,4], Yonghui Xie[2,4], Bingcheng Zhou[3], Zhijiang Wang[2], Dekai Ning[2], Hongming Li[2], Junzheng Zhang[1], Meizhen Yin[3], Jie Shen[1] & Shuo Yan[1]

Tobacco mosaic virus (TMV) is extremely pathogenic and resistant to stress There are great needs to develop methods to reduce the virus in the environment and induce plant immunity simultaneously. Here, we report a multifunctional nano-protectant to reduce the virus in the environment and induce plant immunity simultaneously. The star polycation (SPc) nanocarrier can act as an active ingredient to interact with virus coat protein via electrostatic interaction, which reduces the proportion of TMV particles to 2.9% and leads to a reduction of the amount of virus in the environment by half. SPc can act as an adjuvant to spontaneously assemble with an immune inducer lentinan (LNT) through hydrogen bonding into nanoscale (142 nm diameter) LNT/SPc complex, which improves the physicochemical property of LNT for better wetting performance on leaves and cellular uptake, and further activates plant immune responses. Finally, the LNT/SPc complex displays preventive and curative effects on TMV disease, reducing TMV-GFP relative expression by 26% in the laboratory and achieving 82% control efficacy in the field We hope the strategy reported here would be useful for control of crop virus disease.

As a destructive RNA virus with exceptionally broad host range, tobacco mosaic virus (TMV) infects more than 350 plant species, and the infection remarkably affects crop yield and quality to lead to substantial economic losses estimated at $2.5 billion annually worldwide[1]. TMV disease is regarded as plant cancer, which is difficult to control due to the inherent stability and readily transmission of TMV. More specifically, TMV particles have the strong adaptability toward environmental stress, and are able to survive and remain infection for years, even decades in the environment[2,3]. The virus is readily transmitted via various means such as soil, plant debris and seed, and any minor damage to plants provides an entry point for TMV infection, further complicating the control efforts[3–7]. Thus, there are no effective measures that can absolutely inhibit TMV once it infects plants, and its ubiquitous presence in environment makes complete eradication challenging[8,9].

Current agricultural practices for controlling TMV disease rely on a multi-faceted approach, encompassing seed disinfection, application of plant immune inducers, crop rotation and removal of plant debris[6,10,11]. These strategies primarily focus on two key aspects: reducing environmental reservoirs of TMV particles and bolstering plant immunity. However, the actual control efficacy of existing agents for inactivating environmental virus particles remains very limited[12]. For instance, the compounds isolated from *Aspergillus versicolor* display higher inactivation efficiencies than ningnanmycin, but their inactivation efficiency is merely 50% at 50 μg/mL[13]. The other promising avenue lies in the application of plant immune

[1]Department of Plant Biosecurity, College of Plant Protection, China Agricultural University, 100193 Beijing, China. [2]Kunming Branch of Yunnan Provincial Tobacco Company, 650051 Kunming, China. [3]State Key Laboratory of Chemical Resource Engineering, Beijing Lab of Biomedical Materials, Beijing University of Chemical Technology, 100029 Beijing, China. [4]These authors contributed equally: Qinhong Jiang, Yonghui Xie. e-mail: shenjie@cau.edu.cn; yanshuo2011@foxmail.com

inducers, which can trigger systemic acquired resistance (SAR) in plants, and display broad-spectrum resistance to various plant pathogens[14]. For instance, the salicylic acid (SA), chitosan and lentinan (LNT) stimulate the production of antiviral molecules in plants, thus inhibiting viral replication and providing a protection rate of approximately 60% to 90%[10,15,16]. Some immune inducers even exhibit the ability to directly inactivate viruses, curtailing the spread and severity of virus infection[17]. However, the translocation of immune inducers into plant cells is limited to constrain their control efficacies. Thus, novel technologies should be introduced to improve the bioactivity of inactivation agents and immune inducers to meet the actual demands.

Recently, nanotechnology has shown great potential in delivering various drugs to overcome their limitations, which offers a strategy for the sustainable management of virus diseases[18,19]. The main research directions of nanomaterials in virus disease control include: (1) Nanomaterials can act as active ingredients (AIs) to directly inactivate the viruses. Nanomaterials interact with virus particles through various mechanisms, leading to the physical adsorption or chemical interactions that render virus inactive. For example, kaolin-containing metals nanoparticles (Ag or CuO) show a reduction of viral infectivity close to 99% in the first 10 min of contact of vesicular stomatitis virus (VSV)[20]. Certain nanomaterials, such as carbon nanotubes and graphenes, possess strong surface adsorption capabilities, allowing them to adsorb virus and inactivate virus[21]. (2) Nanomaterials can act as carriers/adjuvants for drugs to improve their bioactivity. For instance, nanocarriers can deliver drugs to virus-infected sites, thus improving drug targeting and bioavailability[22,23]. Moreover, nanocarriers can increase the stability and release period of plant immune inducers, thus prolonging their control efficacy[24]. Our group has designed and developed a low-cost nanocarrier, star polycation (SPc), which exhibits excellent intracellular delivery efficiency, good biocompatibility and biodegradability[25,26]. The SPc contains multiple acceptors and donors for hydrogen bonding, and its positively-charged tertiary amine groups can bind with negatively-charged nucleic acids[27,28]. LNT is a polysaccharide extracted from the fruiting body of *Lentinus edodes*, which has both immune-stimulating and virus-inactivating effects in the management of viral diseases[10,29]. Whether the SPc can serve as a nanocarrier/adjuvant for LNT to amplify the plant defence responses while simultaneously exhibiting excellent inactivation effects on virus particles is an interesting question.

In this study, we design and develop a nanoscale LNT/SPc complex by assembling LNT with SPc nanocarrier. The LNT/SPc complex inactivates TMV particles and reduces viral load in tobacco BY2 cells, seedlings, and soil. The LNT/SPc complex also enhances the plant's defence by improving leaf wetting performance, cellular uptake and activating key resistance-related genes. Biological indicators, such as increased levels of SA, SOD and CAT, confirm the amplification of plant immune responses. In both laboratory and field trial, the LNT/SPc complex exhibits superior preventive and curative effects on TMV compared to LNT alone. This study highlights the SPc nanocarrier's dual role as both active ingredient and adjuvant for LNT and provides a scalable and effective strategy for controlling plant viral diseases.

Results and discussion

Synthesis of SPc

In this study, the star initiator Pt-Br was synthesized from commercially available pentaerythritol with a high yield. The structure of Pt-Br was confirmed by ^{1}H NMR analysis (Supplementary Fig. 1a). Polymerization with 2-(Dimethyl amino) ethyl methacrylate (DMAEMA) was carried out under a nitrogen atmosphere to prevent catalyst deactivation. After polymerization, the solvent (THF) was removed using a rotary evaporator and reused in subsequent cycles, enhancing cost efficiency. The crude product was purified by dialysis in pure water to remove residual DMAEMA, copper and N,N,N′,N′,N″-pentamethyl diethylenetriamine (PMDETA). The final product SPc was obtained as a white powder after freeze-drying. The structure of SPc polymer was confirmed by ^{1}H NMR (Supplementary Fig. 1b).

Self-assembly of nanoscale LNT/SPc complex via hydrogen bonding

The ITC data suggested that the SPc could assemble with LNT spontaneously due to the negative value of Gibbs free energy change (ΔG, −40.28 kJ/mol), and the high affinity constant (Ka) and low dissociation constant (K_d) further demonstrated that this spontaneous complexation was strong (Fig. 1a). Moreover, both negative values of reaction enthalpy (ΔH, −100 kJ/mol) and entropy change (ΔS, −200.3 J/mol·K) indicated that the dominate interaction force between SPc and LNT was hydrogen bonding. Consistent with ITC data, the infrared spectroscopy of LNT/SPc complex exhibited broadening and intensification of peaks around 3500 cm^{-1} compared to those of SPc and LNT, confirming the presence of extensive hydrogen bonding between SPc and LNT (Fig. 1b). It was deduced that the hydroxyl groups in LNT and carbonyl or amidogen groups in SPc formed the hydrogen bonding (Fig. 1c).

We clarified the preparation and self-assembly mechanism of the nanoscale LNT/SPc complex. The SPc is regarded as a versatile nanocarrier for drug delivery due to its unique structural properties. It consists of hydrophobic core and hydrophilic shell, which provide both donors and acceptors for hydrogen bonding. A previous publication has shown that the formation of spirotetramat/SPc complex is also driven by hydrogen bonding, and the possible interaction sites are the amide NH of spirotetramat with carbonyl group or tertiary amines of SPc[30]. Similarly, the tertiary amines of SPc can also assemble with oxhydryl groups of chitosan via hydrogen bonding to form chitosan/SPc complex[31]. Moreover, the positively-charged tertiary amine in the side chain of SPc can be complexed with the negatively-charged oxygen group in osthole via electrostatic interaction[32]. Thus, the SPc is an effective carrier with a lot of potential for various AIs and has a great potential in agricultural applications.

The LNT formed relatively large particles (341 nm) in aqueous solution, and its assembly with SPc broke the self-aggregated structure of LNT and decreased its particle size down to 142 nm (Fig. 1d and Supplementary Table 1). The polydispersities of LNT and LNT/SPc complex were both 0.28, indicating their excellent dispersion in water. Furthermore, the LNT was negatively charged with the zeta potential of −43 mV, and the electrical property turned to positive after its assembly with SPc (Fig. 1e). Both TEM and SEM images revealed that most LNT was comprised of nearly spherical particles, which changed to more regular spheres with smaller particle size after the complexation (Fig. 1d and Supplementary Fig. 2). The SPc disrupted the self-aggregated structure of LNT to form spherical nanoparticles with uniform nanoscale size. In addition, the LNT/SPc complex displayed good dispersibility, which was beneficial for improving its physicochemical properties. The complexation with SPc usually break the self-aggregated large particles of drugs/pesticides in aqueous solution, and aid them to form smaller particles with better bioactivity. For instance, the self-assembly of matrine with SPc decreases the particle size of matrine down to approximately 10 nm, and the matrine/SPc complex exhibits higher cytotoxicity toward S2 cells and stronger lethal effect on green peach aphids[33]. Similarly, the particle size of thiophanate-methyl can be decreased from 834 to 86 nm with the aid of SPc, and thiophanate-methyl/SPc complex displays better inhibition effect on *Verticillium dahliae*[34]. The SPc-loaded fluopyram with smaller particle size also exhibits higher bioactivity against root-knot nematodes with the lethal concentration 50 (LC_{50}) value reduction from 8.63 to 5.70 mg/L[35]. Thus, the SPc can deliver various

https://doi.org/10.1038/s41467-024-52851-z

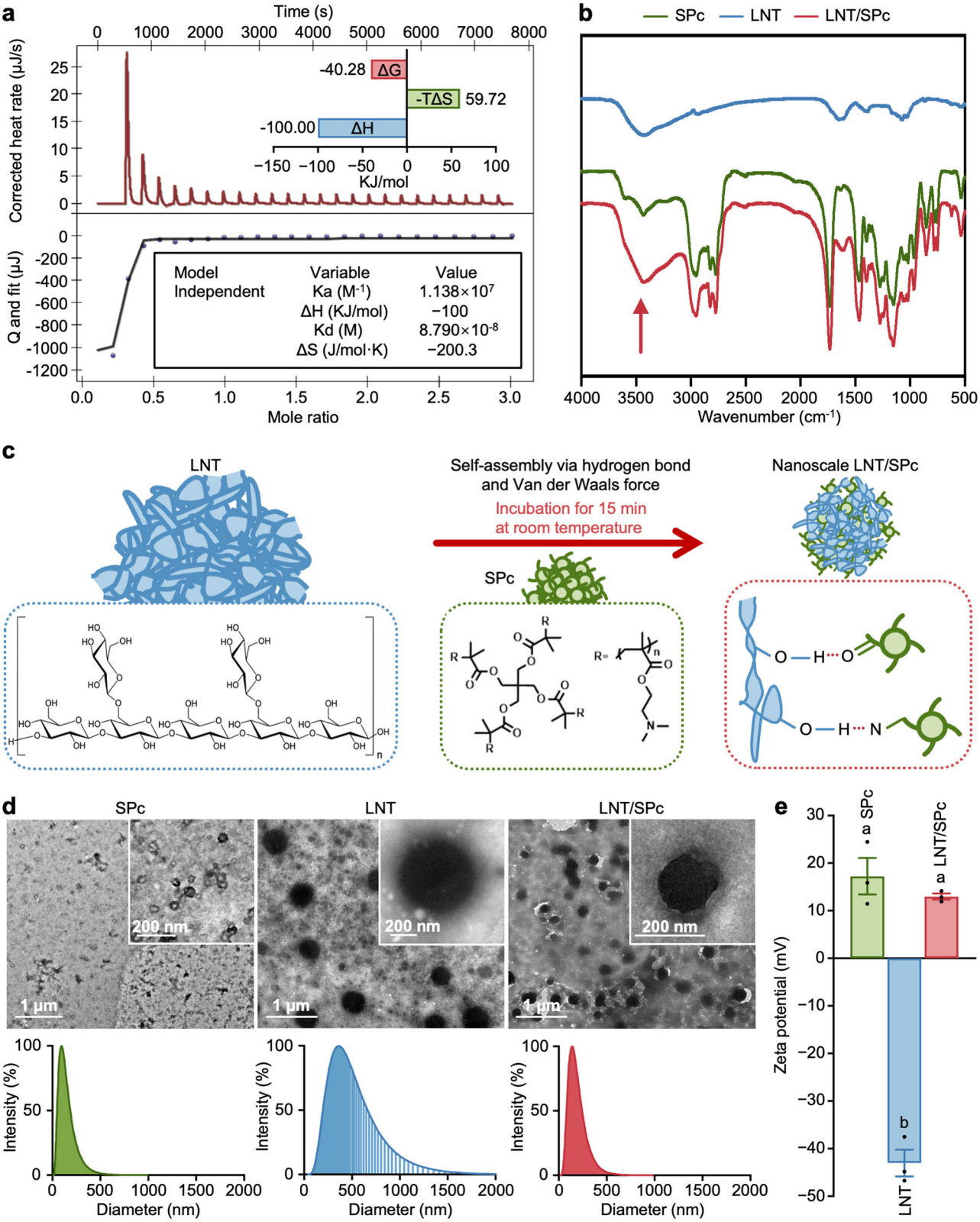

Fig. 1 | Self-assembly mechanism and characterization of LNT/SPc complex. **a** ITC titration of SPc aqueous solution (0.1 mmol/L) into LNT aqueous solution (0.01 mmol/L). **b** Infrared spectra of SPc, LNT and LNT/SPc complex investigated by FTIR. **c** Schematic illustration of self-assembled LNT/SPc complex. **d** TEM images and particle size distributions of SPc, LNT and LNT/SPc complex. **e** Zeta potentials of SPc, LNT and LNT/SPc complex. Each treatment contained three independent samples. Different letters above each bar indicate significant differences at $p < 0.05$ as determined by one-way ANOVA with Tukey HSD test ($F_{2,6} = 148.10$, $p < 0.001$). Bars represent the mean ± SEM. Source data are provided as a Source Data file.

https://doi.org/10.1038/s41467-024-52851-z

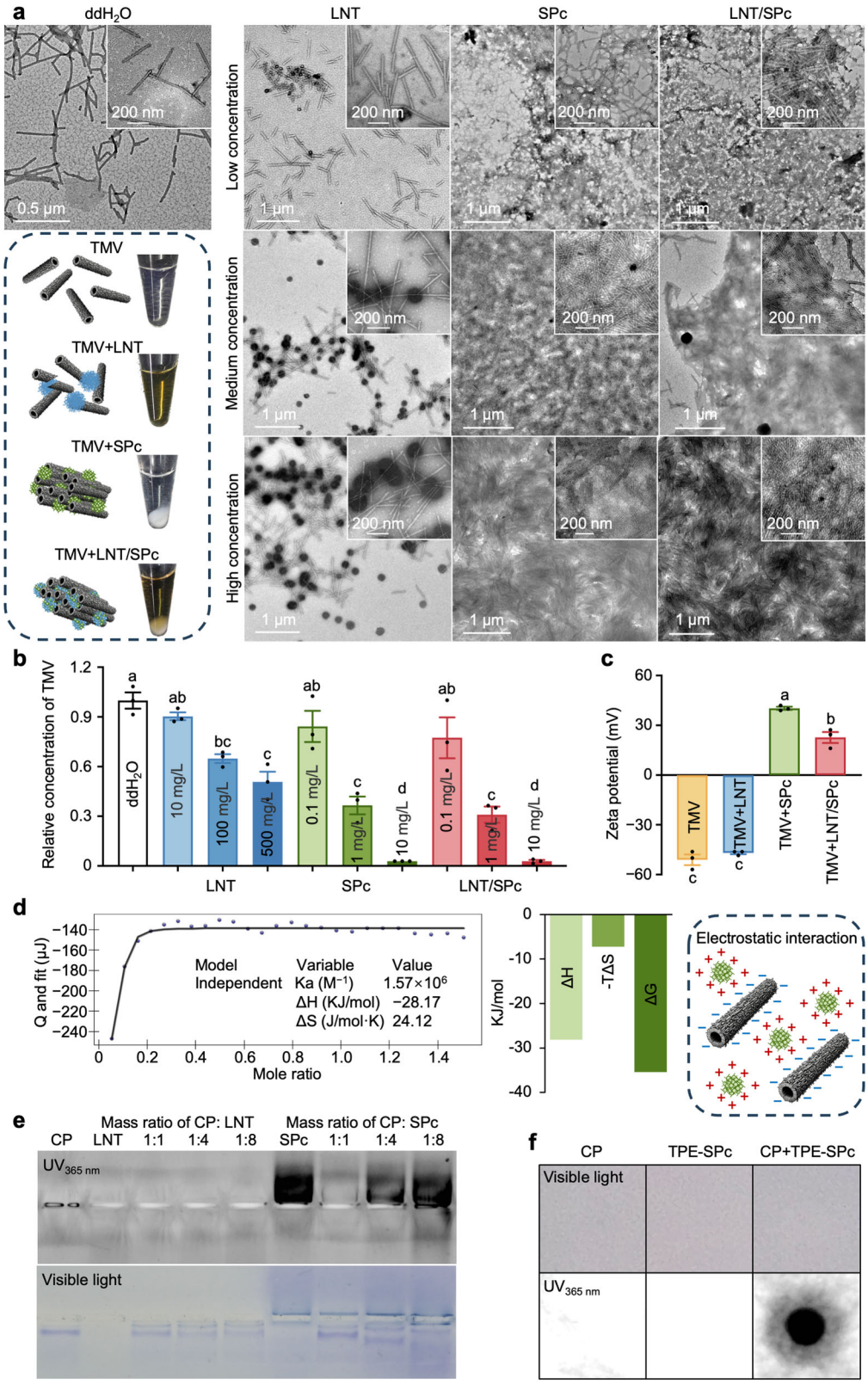

insecticides/fungicides/nematicides to decrease their particle sizes in aqueous solution, which is able to increase their contact area on harmful organisms for better control effects.

SPc-mediated TMV inactivation via electrostatic interaction

The incubation of TMV particles with SPc or LNT/SPc complex led to the formation of obvious white precipitates, and the morphology of TMV particles incubated with the solution of LNT, SPc or LNT/SPc complex was further observed using TEM (Fig. 2a). Representative images showed that most LNT was bound to TMV particles, and the SPc or LNT/SPc complex at lower concentrations could induce the strong aggregation of TMV particles. Moreover, this aggregation phenomenon was more obvious as the concentration of SPc or LNT/SPc complex increased. The aggregation of TMV particles resulted in its

Fig. 2 | Inactivation mechanism of TMV particles by SPc. a TEM images of TMV particles (50 μg/mL) incubated with LNT (10, 100 and 500 mg/L), SPc (0.1, 1, and 10 mg/L) and LNT/SPc complex (0.1, 1 and 10 mg/L) for 6 h, respectively. The schematic illustration of TMV particle inactivation by SPc, LNT or LNT/SPc complex. **b** Relative concentration of TMV incubated with above solutions via qRT-PCR. Relative biomass was quantified (n = 3 biological replicates). Different letters above each bar indicate significant differences at $p < 0.05$ as determined by one-way ANOVA with Tukey HSD test ($F_{9, 20} = 33.51$, $p < 0.001$). Bars represent the mean ± SEM. **c** Zeta potentials of TMV, TMV + LNT, TMV+SPc and TMV + LNT/SPc complex. Each treatment contained three independent samples. Different letters above each bar indicate significant differences at $p < 0.05$ as determined by one-way ANOVA with Tukey HSD test ($F_{3, 8} = 394.00$, $p < 0.001$). Bars represent the mean ± SEM. **d** ITC titration of TMV particle aqueous solution (0.5 mmol/L) into SPc aqueous solution (0.1 mmol/L). The schematic illustration of electrostatic interaction is provided. **e** Native-PAGE images recorded under $UV_{365\ nm}$ or visible light for confirming the interaction between CP protein with LNT or TPE-SPc. The experiment was repeated three times, and a representative Native-PAGE image was shown. **f** Dot blotting assay for the effective binding of CP protein and TPE-SPc. Images were recorded under visible or $UV_{365\ nm}$ light. Source data are provided as a Source Data file.

disintegration to release the naked RNA. Thus, the RNase A was used to degrade the naked RNA released from TMV particles, and the TMV content could be further quantified using qRT-PCR based on the standard curve (Supplementary Fig. 3). The qRT-PCR results demonstrated that the proportions of intact TMV particles decreased to 36.6% and 2.9% after the incubation with 1 and 10 mg/L SPc solution, respectively. Above remained TMV particles were remarkably lower than those treated with 500 mg/L LNT solution (50.9%) (Fig. 2b). Due to the strong effect of SPc, the inactivation effect of LNT/SPc complex was comparable to those of SPc alone.

The current results revealed that the SPc could directly inactivate TMV particles as a more efficient AI compared to LNT. The low concentration of SPc exhibited a better inactivation effect on TMV particles compared to the high concentration of LNT. The obvious aggregation of TMV particles was observed after the incubation with SPc or LNT/SPc complex at the concentration of 1 mg/L, and nearly no TMV particles could survive under the concentration of 10 mg/L. The morphology of TMV particles incubated with LNT was different from that with SPc or LNT/SPc complex. Most LNT were bond to TMV particles, and only high concentration (500 mg/L) of LNT could decrease the amount of TMV particles. A similar publication has reported that a polysaccharide isolated from Chinese fungus (Yun Chi) has inactivation effects on TMV particles by gathering up and destroying TMV particles[36]. The current results confirmed the antiviral activity of SPc against TMV particles, and we deduced that this bio-toxicity was relatively specific to virus. Previous studies have confirmed the good biocompatibility of SPc toward model insect *Drosophila melanogaster*, predatory insect *Harmonia axyridis* and *Picromerus lewisi*, fungus *V. dahliae*, and nematode *Meloidogyne enterolobii*[34,37,38]. Only high concentrations of SPc can lead to the death of *H. axyridis* larvae with LC_{50} values of 43.96 and 19.85 mg/mL via soaking and oral feeding methods, respectively[37]. Thus, the high bio-toxicity of SPc was firstly observed toward TMV particles, and its mechanism was investigated in the following experiment.

To examine the interaction between TMV particles with various solutions, the TMV particles were titrated with the solution of LNT, SPc or LNT/SPc complex to examine the thermodynamic parameters. The ITC data revealed that the LNT was bound to TMV particles via hydrogen bonding due to the negative values of ΔH and ΔS (Supplementary Fig. 4a). The coat protein (CP) of TMV particles was constructed, and its docking with LNT molecules was simulated, which revealed that the serine-16, serine-50, tryptophan-53 and arginine-72 in CP protein might act as important roles in hydrogen bonding (Supplementary Fig. 4b). Interestingly, the ITC data demonstrated that the interaction of TMV particles with SPc or LNT/SPc complex was different from that with LNT alone, and the negative value of ΔH and positive value of ΔS suggested that the TMV particles could spontaneously bind to SPc or LNT/SPc complex through electrostatic interaction (Fig. 2d and Supplementary Fig. 4c). Meanwhile, the zeta potential results also supported above conclusion (Fig. 2c). The TMV particles and their mixture with LNT carried negative charges, whereas the mixtures of TMV + SPc and TMV + LNT/SPc complex were positively charged.

To further confirm the interaction between TMV particles with SPc, the CP protein of TMV particles was expressed and purified (Supplementary Fig. 5), and the CP protein was incubated with TPE-SPc (Modified fluorescent SPc that could be detected at 365 nm) at various mass ratios for native-PAGE assay. In native-PAGE gel, multiple bands would be seen if the CP protein has polymerized forms with LNT or TPE-SPc. The CP protein and TPE-SPc alone migrated toward the anode and cathode under the electric field, respectively (Fig. 2e). With the addition of LNT or TPE-SPc, two bands could be seen in the gel in which the stronger staining band indicating the CP protein position. The addition of TPE-SPc caused the band of CP protein to become fainter and shift position. Meanwhile, the TPE-SPc was applied to perform a dot-blot assay on positively charged nylon membranes. The negatively charged CP protein caused the accumulation of TPE-SPc at protein spots, indicating the effective interaction between CP protein and SPc (Fig. 2f).

The LNT could interact with TMV particles via hydrogen bonding, whereas the interaction force of TMV particles with SPc or LNT/SPc complex turned to electrostatic interaction, which was due to the different charge properties of TMV particles, LNT and SPc. Both TMV particles and LNT were negative-charged, and the SPc and LNT/SPc complex were positive-charged. Thus, the interaction force of TMV particles with LNT was different from that with SPc or LNT/SPc complex. Furthermore, the native-PAGE and dot-blot results demonstrated that the effective binding of SPc with TMV CP protein caused the aggregation of TMV particles and disrupted the intact structure of TMV particles. There are three primary mechanisms of virus inactivation by nanomaterials[39,40]. (1) Nanomaterials can impede viral interaction with host cells via the formation of physical barriers on the surface of host cells, thereby preventing the virus–cell contact. (2) Nanomaterials can also obstruct viral entry into host cells by binding with viral envelope proteins. (3) Nanomaterials can directly disrupt viruses by releasing ROS or employing alternative mechanisms. The current study revealed that the SPc could bind with the CP protein, which in turn disrupted the TMV particles. Similar inactivation effects against TMV particles have also been observed with zinc oxide nanoparticles (ZnONPs), which can directly bind to TMV particles to cause their substantial aggregation and breakage[29]. A water-borne sprayable nanomaterial can effectively bind to the membrane of SARS-CoV-2 and subsequently disrupt it via nanoscale conformational changes, leading to the degradation of viral RNA[41].

Efficient inactivation of TMV particles by LNT/SPc complex

The inactivation effects of LNT/SPc complex on TMV particles in tobacco cells, seedlings and soil were evaluated in the current study. The GFP-tagged TMV (TMV-GFP) or TMV particles were incubated with LNT, SPc, or LNT/SPc complex, mixed with tobacco BY-2 cells, and then ultrasonicated and cultured for 24 h. Subsequently, the green fluorescence from TMV-GFP particles was detected, and the TMV-GFP and TMV particles were quantified using qRT-PCR (Fig. 3a). There was nearly no fluorescent signal detected in the cells treated with TMV + SPc or TMV + LNT/SPc complex, compared to strong fluorescent intensity in the cells treated with TMV or TMV + LNT. Similarly, the

https://doi.org/10.1038/s41467-024-52851-z

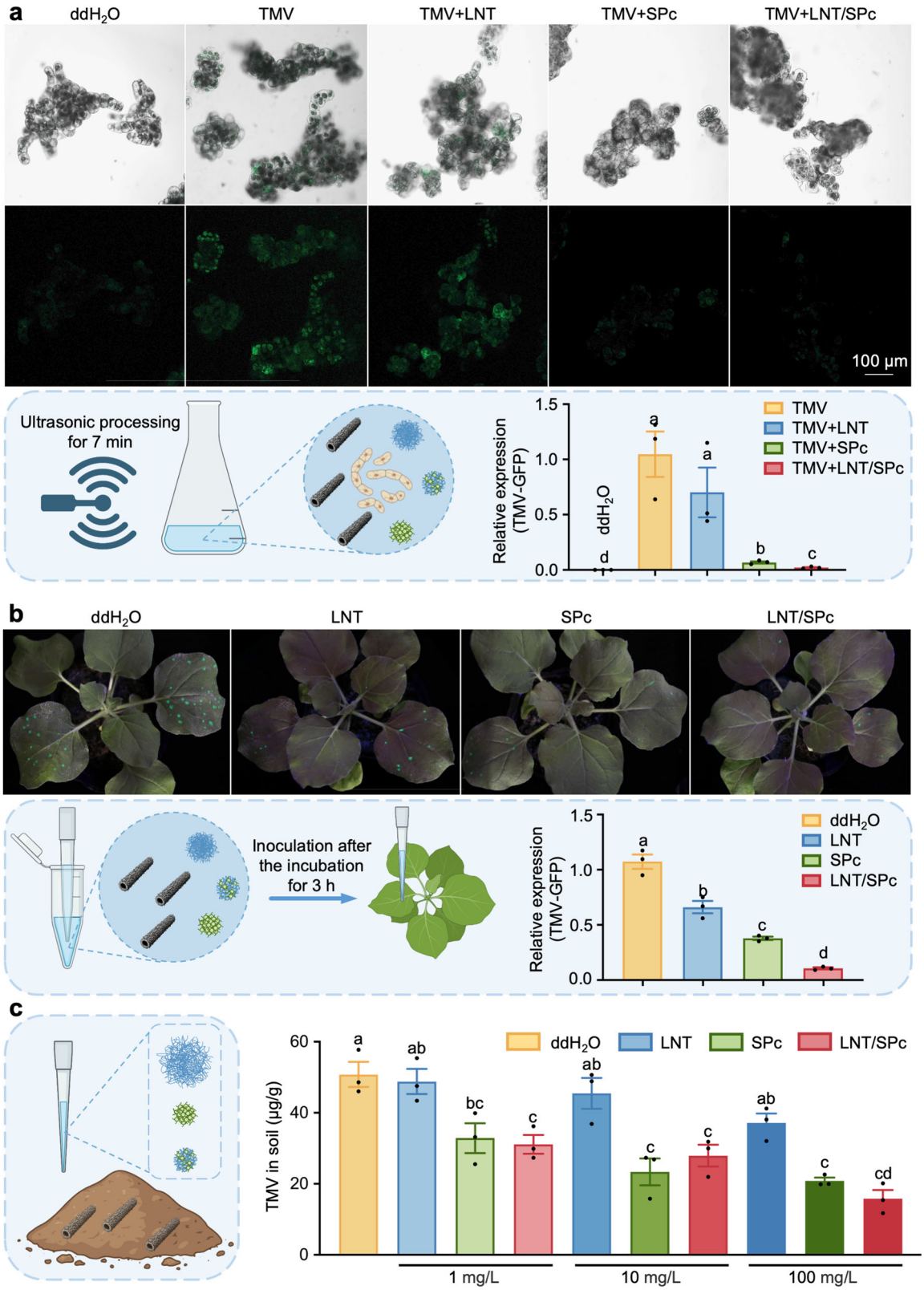

relative expression of TMV-GFP decreased to 6.9% and 2.1%, and that of TMV decreased to 0.79% and 0.74% in the cells treated with TMV + SPc and TMV + LNT/SPc complex, respectively (Supplementary Fig. 6). The above results demonstrated that the SPc or LNT/SPc complex exhibited strong inactivation effects on TMV. However, the inactivation effect of LNT alone was much weaker, with TMV-GFP relative expression reducing to 70.2% and TMV relative expression reducing to 87.2%.

The TMV-GFP particles were incubated with LNT, SPc or LNT/SPc complex, and the mixtures were inoculated on tobacco seedlings. The inactivation effects of various treatments were examined at 3 d post-inoculation. Compared to the leaves treated with double distilled water (ddH_2O), the leaves treated with LNT had fewer green-fluorescent spots, and nearly no green-fluorescent spots were observed on the leaves treated with SPc or LNT/SPc complex (Fig. 3b).

Fig. 3 | Strong inactivation of TMV particles by LNT/SPc complex. a Inactivation efficacies of LNT (100 mg/L), SPc and LNT/SPc complex against TMV particles (50 μg/mL) in tobacco cells. The representative fluorescent images of BY2 cells were taken, and TMV-GFP relative expression was quantified via qRT-PCR at 24 h after the incubation. Relative biomass was quantified ($n = 3$ biological replicates). Different letters above each bar indicate significant differences at $p < 0.05$ as determined by one-way ANOVA with Tukey HSD test ($F_{4, 10} = 12.22$, $p = 0.007$). Bars represent the mean ± SEM. **b** Inactivation efficacies of LNT (100 mg/L), SPc and LNT/SPc complex against TMV particles (50 μg/mL) in tobacco seedlings. The representative fluorescent images were taken, and TMV-GFP relative expression was quantified via qRT-PCR at 3 dpi. Relative biomass was quantified ($n = 3$ biological replicates). Different letters above each bar indicate significant differences at $p < 0.05$ as determined by one-way ANOVA with Tukey HSD test ($F_{3, 8} = 88.74$, $p < 0.001$). Bars represent the mean ± SEM. **c** Inactivation efficacies of LNT (100 mg/L), SPc and LNT/SPc complex against TMV particles (50 μg/mL) in soil. The TMV expression was quantified via qRT-PCR at 12 h after the incubation. Relative biomass was quantified (n = 3 biological replicates). Different letters above each bar indicate significant differences at $p < 0.05$ as determined by one-way ANOVA with Tukey HSD test ($F_{9, 20} = 13.71$, $p < 0.001$). Bars represent the mean ± SEM. Source data are provided as a Source Data file.

Similarly, the qRT-PCR results also indicated that there were less TMV-GFP particles in the leaves treated with SPc or LNT/SPc complex, and their relative expression of TMV-GFP decreased to 37.9% and 10.7%, respectively. As expected, the LNT treatment also decreased the amount of TMV particles in leaves.

In the current study, the TMV particles were mixed with soil, and treated with LNT, SPc or LNT/SPc complex, and the amount of TMV particles was quantified using qRT-PCR based on the standard curve (Supplementary Fig. 7). The application of SPc or LNT/SPc complex could decrease the amount of TMV particles in soil, and the amount of TMV particles decreased to 32.9 and 31.1 μg/g after the treatment with SPc (1 mg/L) and LNT/SPc complex, respectively (Fig. 3c). Notably, the amount of TMV particles could be reduced to 15.8 μg/g after the treatment with LNT/SPc complex (100 mg/L). The application of LNT alone could also decrease the amount of TMV particles in soil, however there was no significant difference compared with the control group (ddH_2O).

The LNT/SPc complex or SPc displayed excellent inactivation effects on TMV particles in tobacco cells and seedlings. The amounts of TMV particles could be decreased in tobacco BY2 cells and seedlings treated with SPc or LNT/SPc complex. A previous study has reported the inactivation effects of LNT on infectious hematopoietic necrosis virus (IHNV)[42]. The LNT is mixed with IHNV particles and incubated with *Epithelioma papulosum cyprini* (EPC) cells, and the antiviral activity reaches 62.34%. However, the inactivation effect of LNT alone is relatively weak due to its limited contact to TMV particles in the field. As one of the most stable viruses in the environment, TMV can spread via soil, seeds, agricultural practices, etc[6,43,44]. For instance, TMV can spread through plant root tips in soil-circulating water systems, and its long persistence in soil usually facilities the transmission among various host plants[45]. Thus, the inactivation effect of TMV particles by LNT/SPc complex was evaluated in the soil. The current study revealed that the application of SPc or LNT/SPc complex could reduce the amount of TMV particles in the soil. Whereas, the LNT alone displayed very limited inactivation effects. Continuous field application of LNT/SPc complex was expected to reduce the amount of TMV particles in the soil, which held significant implications for long-term management of TMV.

Amplified plant defence induced by SPc-loaded LNT

The contact angle and retention of pesticide droplets can reflect the wetting performance on leaf surface, which are related with the plant uptake and control efficacy. With the aid of SPc, the contact angle of LNT decreased from 87.4° to 82.7°, and its retention increased from 8.6 to 12.7 mg/cm², indicating the better wetting performance of LNT/SPc complex on tobacco leaves (Fig. 4a). Meanwhile, the fluorescein isothiocyanate (FITC) was used to stain the LNT to prepare the fluorescent FITC-LNT, and tobacco BY2 cells were incubated with SPc-loaded FITC-LNT. The fluorescent intensity was remarkably higher in the cells incubated with SPc-loaded FITC-LNT compared to that with FITC-LNT alone, indicating that the application of SPc could facilitate the rapid cellular uptake of FITC-LNT (Fig. 4b).

In spite of the inactivation effects, the SPc could also act as an efficient nanocarrier/adjuvant to enhance the wetting performance of LNT and improve its plant uptake to amplify the plant defence responses. In the current study, the electrical property of LNT turned to positive charge after the assembly with SPc, which could improve the affinity of LNT to tobacco leaves. A previous study has reported that a positively-charged nanomaterial (PS-NH_2) is tended to associate with the leaf surfaces than a negatively-charged nanomaterial (PS-COOH)[46]. As expected, the contact angle of SPc-loaded LNT decreased, and its retention increased, which were crucial for the plant uptake of drugs sprayed onto leaf surfaces[47,48]. However, it was difficult to detect the plant uptake of LNT due to the large molecular weight of polysaccharides. Our previous studies have demonstrated that the plant uptake of pesticides can be improved with the aid of SPc. For instance, the SPc can remarkably promote the plant uptake of imidaclothiz by 2.94–4.00 times, which is related to the smaller particle size and contact angle of imidaclothiz/SPc complex[49]. The plant uptake of SPc-delivered thiamethoxam is also increased by 1.69-1.84 times compared with thiamethoxam alone[50]. Our results demonstrated that the cellular uptake of LNT was remarkably improved with the aid of SPc, and the enhanced delivery is related with the activation of clathrin-mediated endocytosis by SPc, which can accelerate the plant and cellular uptake[51,52].

To investigate the plant defence induced by LNT/SPc complex, the RNA-seq analysis was performed using the tobacco seedlings sprayed with LNT and LNT/SPc complex. The quality and correlation of RNA-seq samples were good for the following experiments (Supplementary Table 2 and Supplementary Fig. 8). RNA-seq results showed that there were 555 differentially expressed genes (DEGs), of which 341 genes were up-regulated and 214 genes were down-regulated in the seedlings treated with LNT/SPc complex compared to LNT alone (Fig. 5b). Kyoto Encyclopedia of Genes and Genomes (KEGG) analysis indicated that the DEGs were enriched in multiple signaling pathways related to plant-pathogen interaction, plant hormone signal transduction, peroxisome, secondary metabolism, etc. (Fig. 5a). GO analysis further classified the DEGs into three processes, which were primarily related with defence response, extracellular region, peroxidase activity, oxidation-reduction process, etc. More specifically, many genes encoding pathogenesis-related proteins such as *osmotin-like protein* (*OLP*), *pathogenesis-related protein 1* (*PR1*), *pathogenesis-related protein 10* (*PR10*), *pathogenesis-related protein STH-2* (*STH2*) and *pathogenesis-related genes transcriptional activator 5* (*PTI5*) were up-regulated in the seedlings treated with LNT/SPc complex (Fig. 5c). Two genes *protein SRC2* (*SRC2*) and *catalase-1* (*CAT1*) involved in the production and homeostasis of reactive oxygen species (ROS) were also up-regulated.

The RNA-seq results showed that the genes related with defence response, hypersensitive response, oxidative stress response, etc. were up-regulated in the tobacco seedlings treated with LNT/SPc complex compared to LNT alone. For example, *OLP* has a dual function in osmotic stress and plant pathogen defence, which is required for hypersensitive cell death response and oxidative burst signaling[53,54].

https://doi.org/10.1038/s41467-024-52851-z

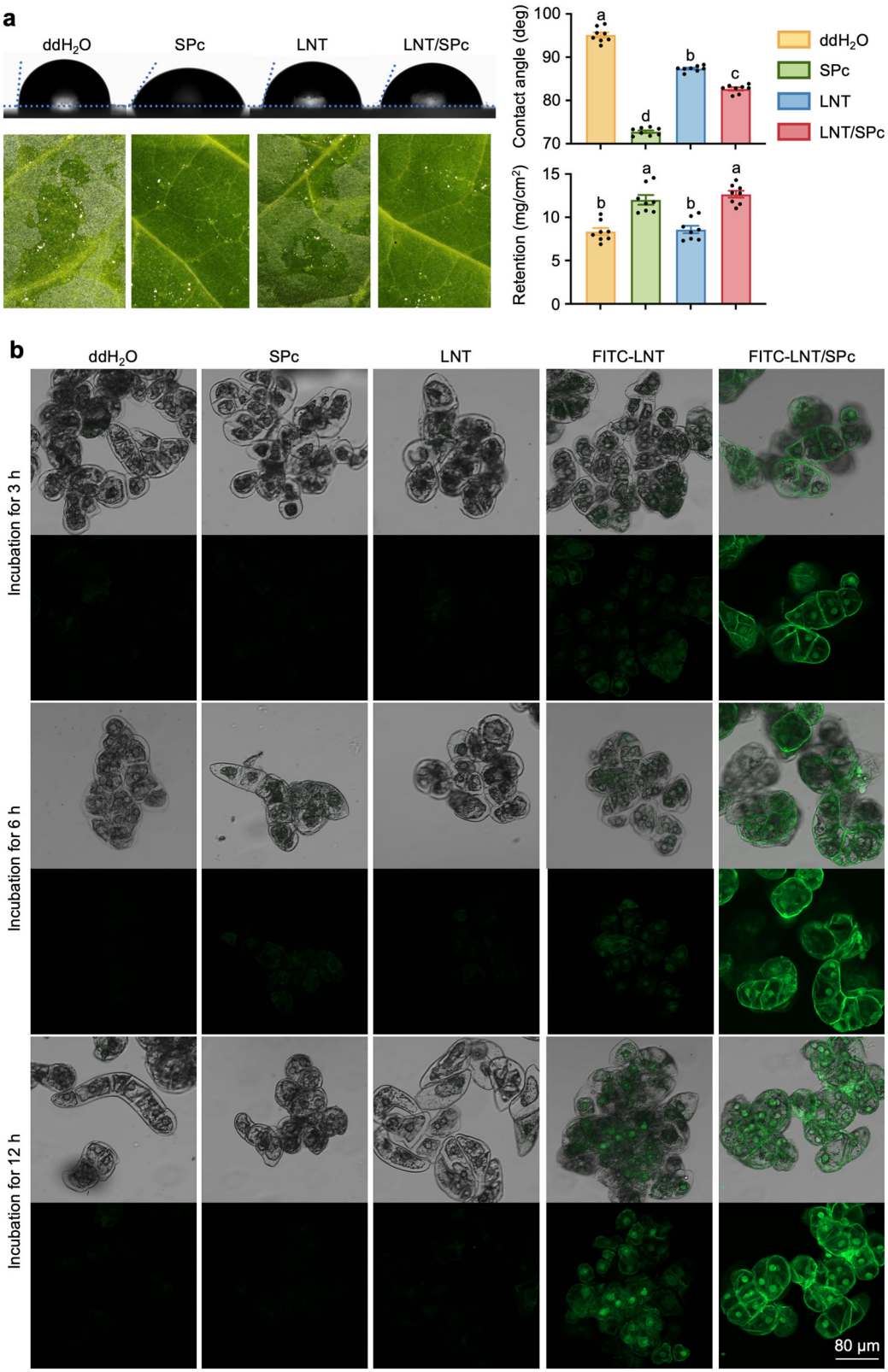

Fig. 4 | Contact angle, retention and cellular uptake of SPc-loaded LNT. **a** Contact angles and retentions of various solutions (H_2O, SPc, LNT and LNT/SPc complex) on the glass slides and tobacco leaves (8 cm^2). The representative images were taken. Relative biomass was quantified ($n = 8$ biological replicates). Different letters above each bar indicate significant differences at $p < 0.05$ as determined by one-way ANOVA with Tukey HSD test (Contact angles: $F_{3, 28} = 543.50$, $p < 0.001$; Retention: $F_{3, 28} = 24.90$, $p < 0.001$). Bars represent the mean ± SEM. **b** Cellular uptake of various solutions (H_2O, SPc, LNT, FITC-LNT and FITC-LNT/SPc complex). The representative fluorescent images of BY2 cells were taken at 3, 6 and 12 h after the incubation, with 5 representative images captured for each treatment. Source data are provided as a Source Data file.

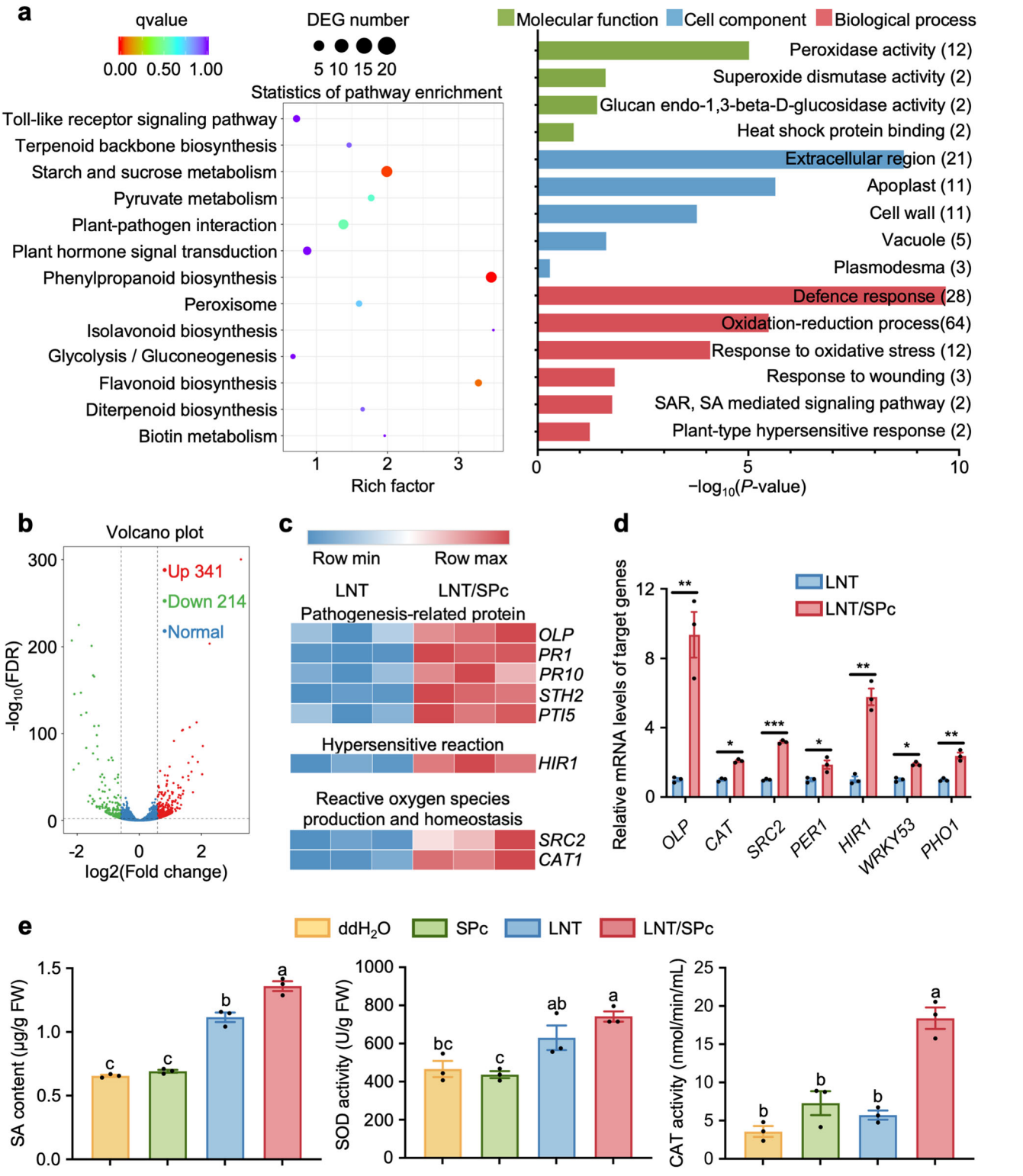

As plant disease resistance proteins, PR proteins have antiviral, antibacterial and antifungal activities, and PR10 can activate the production of SOD, peroxidase (POD) and phenylalanine ammonia lyase (PAL) in plants, which are deposited in plant cell wall for enhancing the defence ability of cell wall and preventing pathogen invasion[55–58]. HIR1 can interact with defence response proteins and regulate plant cell death and immunity[59,60]. SCR2 and CAT1 also mediate the production of ROS and alleviate ROS damage to plant cells to participate in defence response[61–63].

The qRT-PCR was performed to verify the RNA-seq results. The relative expression levels of *OLP*, *HIR1* and *SRC2* increased by 9.3, 5.6 and 3.2 times in the seedlings treated with LNT/SPc complex, which were consistent with the RNA-seq results (Fig. 5d). Subsequently, the plant defence-related substances such as SA, superoxide dismutase (SOD) and catalase (CAT) were detected to confirm the amplified plant defence induced by SPc-loaded LNT based on corresponding standard curves (Supplementary Fig. 9 and Fig. 5e). The application of both LNT and LNT/SPc complex could induce SA production, and the SA

Fig. 5 | Amplified plant defence responses induced by SPc-loaded LNT. a-c RNA-seq analysis to illustrate the plant defence responses induced by LNT/SPc complex. The tobacco seedlings sprayed with the solution of LNT (100 mg/L) or LNT/SPc complex were used to prepare RNA sequencing libraries. **a** KEGG and GO analysis of DEGs. DESeq was used to analyze the DEGs between two treatments, and a fold change of ≥ 2.0 and a false-discovery rate (FDR) of <0.01 were used as the screening conditions. **b** Analysis of DEGs with a volcano plot. **c** Heat maps of DEGs associated with pathogenesis-related protein, hypersensitive reaction, and reactive oxygen species production and homeostasis. Highly expressed genes are shown in red, whereas genes with low expression levels are shown in blue. **d** Validation of DEGs using qRT-PCR. The relative mRNA levels of target genes were normalized to the abundance of the *actin* gene. Relative biomass was quantified (n = 3 biological replicates). The asterisk indicates significant difference according to independent *t* test (two-sided, $^{*}p < 0.05$, $^{**}p < 0.01$ and $^{***}p < 0.001$). *OLP* ($t = 10.69$, df = 2, $p = 0.009$), *CAT* ($t = 8.75$, df = 2, $p = 0.013$), *SRC2* ($t = 83.15$, df = 2, $p < 0.001$), *PER1* ($t = 6.95$, df = 2, $p = 0.020$), *HIR1* ($t = 17.34$, df = 2, $p = 0.003$), *WRKY53* ($t = 8.94$, df = 2, $p = 0.012$) and *PHO1* ($t = 27.44$, df = 2, $p = 0.001$). Bars represent the mean ± SEM. **e** SA content, SOD activity and CAT activity in tobacco seedlings treated with ddH_2O, SPc (100 mg/L), LNT and LNT/SPc complex. Relative biomass was quantified (n = 3 biological replicates). Different letters above each bar indicate significant differences at $p < 0.05$ as determined by one-way ANOVA with Tukey HSD test (SA content: $F_{3,8} = 151.70$, $p < 0.001$; SOD activity: $F_{3,8} = 11.77$, $p = 0.003$; CAT activity: $F_{3,8} = 33.68$, $p < 0.001$). Bars represent the mean ± SEM. Source data are provided as a Source Data file.

concentration increased to 1.36 ug/g FW in the seedlings treated with LNT/SPc complex compared to 1.16 μg/g FW in LNT treatment. Similarly, both LNT and LNT/SPc complex could elevate the SOD activity. The SOD activity in the seedlings treated with LNT/SPc complex was higher than that with LNT alone, but there was no significant difference. The CAT activity (18.41 nmol/min/mL) was the highest in the seedlings treated with LNT/SPc complex among various formulations.

Above results suggested that the SPc could promote the LNT-induced plant antiviral response. As a crucial plant defence-related molecule, the SA activates resistance-related gene expression, regulates cell death to curb pathogen proliferation within plants, induces ROS accumulation, and interacts with other plant hormones such as jasmonic acid and abscisic acid to collectively regulate plant resistance responses[64]. In the current study, the application of SPc increased the SA content in tobacco seedlings induced by LNT. Furthermore, the activities of SOD and CAT were elevated in the seedlings treated with LNT/SPc complex. The SOD and CAT can maintain the balance of intracellular ROS, and elevated activities of SOD and CAT assist the clearance of ROS to reduce the oxidative damage and increase the plant resistance[65,66].

Excellent preventive and curative effects of LNT/SPc complex on TMV

The preventive and curative effects of LNT/SPc complex were firstly evaluated using the tobacco seedlings in laboratory. For preventive effect assay, the tobacco seedlings were sprayed with various formulations and then inoculated with TMV-GFP. Compared to ddH_2O and SPc, the application of both LNT and LNT/SPc complex could reduce the green fluorescence in leaves, and the relative expression of TMV-GFP was 3.03 in the seedlings treated with LNT/SPc complex compared to 4.14 with LNT at 4 d post-inoculation (Fig. 6a). For curative effect assay, the tobacco seedlings were inoculated with TMV-GFP and then sprayed with various formulations. The LNT/SPc complex also displayed the best curative effect on TMV, and the relative expression of TMV-GFP was 4.21 in the seedlings treated with LNT/SPc complex (Fig. 6b).

The LNT/SPc complex exhibited excellent control effects on TMV in field trials (Fig. 6c). The application of LNT or LNT/SPc complex reduced the number of mosaic leaves. The control efficacy of LNT/SPc complex reached 91.5% at 7 d post-application, which was 27.3% higher than that of LNT alone. Notably, the control efficacy of LNT/SPc complex still remained at 81.9% at 14 d post-application compared to merely 31.3% of LNT alone. Furthermore, the tobacco seedlings treated with LNT/SPc complex displayed excellent agronomic traits. Compared to LNT alone, the seedlings treated with LNT/SPc complex were remarkably higher with larger leaves at 14 d post-application (Fig. 6d). Meanwhile, the LNT/SPc complex was relatively safe toward tobacco BY2 cells and seedlings, and no significant adverse impacts were observed after the treatment with LNT/SPc complex (100 mg/L) (Supplementary Fig. 10 and Supplementary Fig. 11).

The LNT/SPc complex exhibited excellent preventive and curative effects on TMV in the laboratory and field. Furthermore, the application of LNT/SPc complex could alleviate the infection symptoms of TMV, and promote the growth of infected tobacco seedlings. Similar to previous studies, the SPc can act as an efficient adjuvant to improve the control efficacies of chitosan, thiophanate-methyl and osthole toward potato late blight, cotton verticillium wilt and strawberry powdery mildew in the field, respectively[31–34]. Interestingly, the application of SPc alone did not show any control efficacy against TMV in the field. The possible reason was that the SPc application was carried out after the infection, and the inactivation effect of SPc against environmental TMV was too late to be achieved. Nevertheless, continuous field application of LNT/SPc complex could reduce TMV particles in the environment, which was beneficial for long-term management of TMV. Apart from field spraying, the multifunctionality of LNT/SPc complex enabled its application in various agricultural scenarios, including seed coating/soaking, floating seedling cultivation, soil treatment, etc. Seed coating/soaking and floating seedling cultivation can inhibit viral transmission among seeds and seedlings, respectively[45,67]. Soil treatment can decrease the presence of virus particles in soil and plant debris[68]. In terms of scalability and economic feasibility, the current synthetic cost of SPc in the laboratory is as low as 14 g/$, with the application amount of approximately 13.5 g per hectare, and the application cost of LNT/SPc complex is 5.78$ per hectare. Additionally, we conducted a successful field demonstration over 150 hectares during 2022 in Yunnan Province (China), and the control efficacy was excellent after the application of LNT/SPc complex three times. The application cost of LNT/SPc complex will be further decreased for mass production in factories. Meanwhile, no adverse effects were observed in tobacco cells and seedlings treated with LNT/SPc complex, revealing its safety in actual application. In summary, our work presented a groundbreaking innovation: the nanomaterial SPc could not only act as a powerful AI to inactivate the TMV particles, but also an efficient nanocarrier/adjuvant to deliver LNT to amplify the plant defence responses. Our findings paved the way for the design and development of nano-protectants with dual-synergistic mechanism for sustainable crop protection.

Methods

Chemical reagents and SPc synthesis

The LNT standard was purchased from Shanghai Yuanye Biochemical Technology Co. (China). Ethanol and methanol were purchased from Sinopharm Chemical Reagent Co. (China). Triethylamine (TEA), DMAEMA and 2-bromo-2-methylpropionyl bromide purchased from Energy Chemical (China), and PMDETA, CuBr and tetrahydrofuran purchased from Sigma-Aldrich (USA) were used to synthesize SPc. Other chemical reagents were obtained from Beijing Chemical Works (China).

The synthesis of SPc was carried out via two reaction steps. Initially, 2-bromo-2-methylpropionyl bromide (253 mg) was incrementally

https://doi.org/10.1038/s41467-024-52851-z

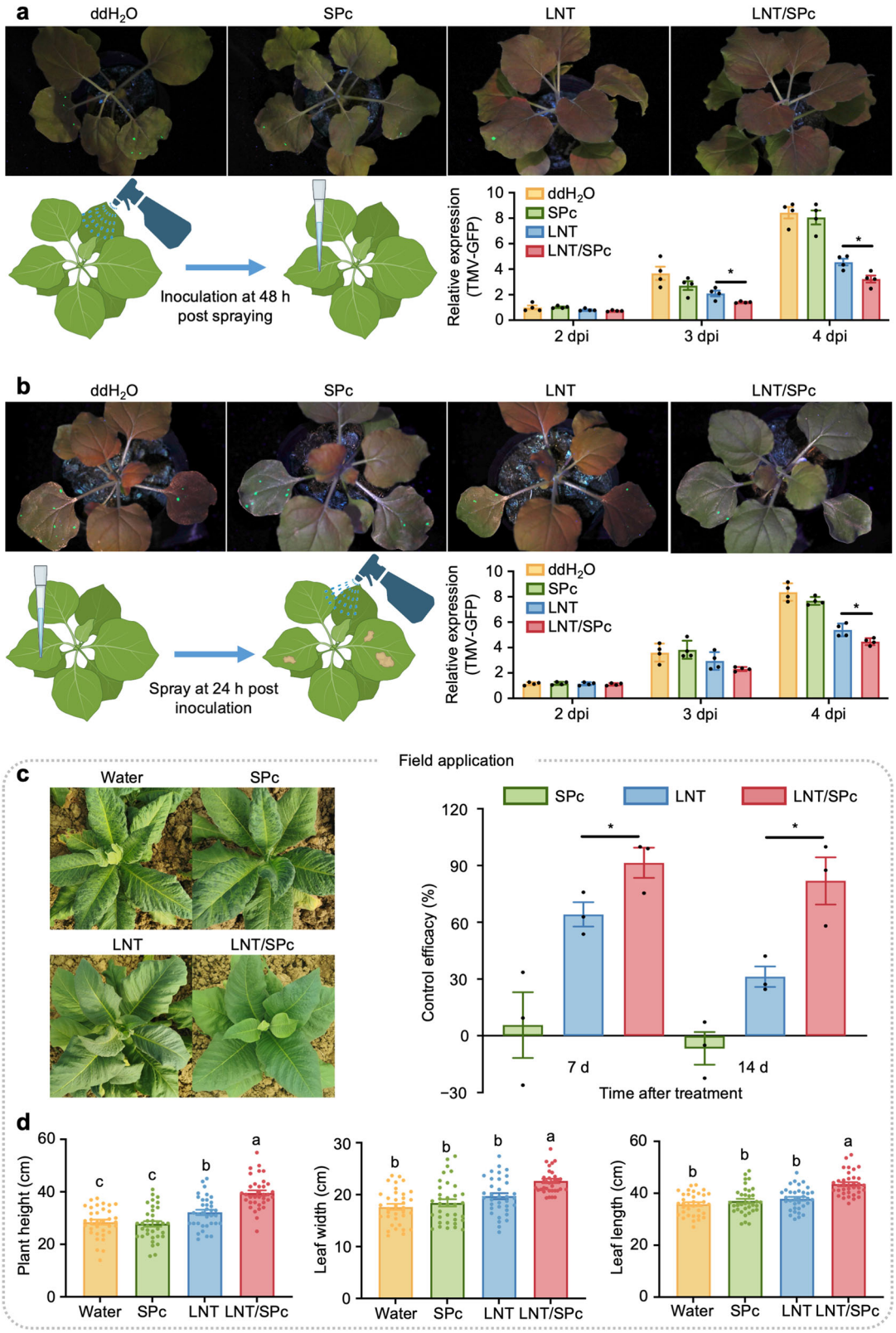

added into the solution of pentaerythritol (25 mg) dissolved in anhydrous tetrahydrofuran (20 mL) with TEA (111.3 mg) under 0 °C. The mixture was stirred for 24 h, and the reaction was terminated by adding methanol. The resultant product underwent recrystallization in cold ether to yield the Pt-Br (50 mg, 40% yield). The structure of Pt-Br was confirmed by ^{1}H NMR (400 MHz, $CDCl_3$). Nuclear magnetic resonance (^{1}H NMR) spectra were recorded at room temperature using a Bruker 400 spectrometer. Subsequent steps involved the conversion of Pt-Br into SPc. A reaction flask, equipped with a magnetic stirrer, was charged with Pt-Br (40 mg), DMAEMA (3.1 g) and anhydrous tetrahydrofuran (8 mL). The mixture was subjected to nitrogen degassing for 30 min to create an inert atmosphere. Thereafter, CuBr (46 mg) and PMDETA (110 mg) were introduced into the flask. The polymerization reaction was then allowed to proceed at 60 °C for 7 h. Finally, the

Fig. 6 | Excellent preventive and curative effects of LNT/SPc complex on TMV. **a** Preventive effect of LNT/SPc complex in the laboratory. Tobacco seedlings were sprayed with LNT (100 mg/L) or LNT/SPc complex, and 50 μL TMV-GFP (20 μg/mL) was inoculated 48 h later. The ddH_2O and SPc were also employed. Biomass was quantified (n = 4 biological replicates, 3 seedlings/replicate). The representative photos were acquired at 3 dpi, and the TMV-GFP relative expression was quantified via qRT-PCR at 2, 3 and 4 dpi. Significant differences indicated by *t* test (two-sided, 3 dpi: $t = 3.06$, df = 6, $p = 0.022$; 4 dpi: $t = 3.44$, df = 6, $p = 0.014$; $^*p < 0.05$). **b** Curative effect of LNT/SPc complex in the laboratory. Seedlings were inoculated with TMV-GFP, then sprayed with LNT (100 mg/L) or LNT/SPc complex after 24 h. Biomass was quantified (n = 4 biological replicates, 3 seedlings/replicate). The representative photos were acquired at 3 dpi, and the TMV-GFP relative expression was quantified by qRT-PCR at 2, 3 and 4 dpi. Significant differences indicated by *t* test (two-sided, $t = 3.20$, df = 6, $p = 0.019$, $^*p < 0.05$). **c** Control efficacy of LNT/SPc complex against TMV in the field. Tobacco seedlings were sprayed with LNT (40 mg/L) and LNT/SPc complex, respectively. The water and SPc were also applied. Each treatment contained three independent plots (Three replicates), and each plot was approximately 240 m^2. The representative photos were taken at 14 d after the treatment. Significant differences indicated by *t* test (two-sided, 7 d: $t = 2.85$, df = 4, $p = 0.047$; 14 d: $t = 3.73$, df = 4, $p = 0.020$, $^*p < 0.05$). **d** Agronomic traits of treated tobacco seedlings at 14 d. Each treatment included 35 randomly-selected seedlings. Different letters above each bar indicate significant differences at $p < 0.05$ as determined by one-way ANOVA with Tukey HSD test (Plant height: $F_{3,\ 136} = 28.05$, $p < 0.001$; Leaf width: $F_{3,\ 136} = 14.35$, $p < 0.001$; Leaf length: $F_{3,\ 136} = 19.42$, $p < 0.001$). **a-d** Bars represent the mean ± SEM. Source data are provided as a Source Data file.

mixture was cooled to room temperature and exposed to air to quench the reaction, and the SPc was obtained as a white powder after freeze-drying. The structure of SPc was also confirmed by ^1H NMR (400 MHz, $CDCl_3$).

ITC and FTIR techniques for self-assembly mechanism of LNT/SPc complex

The dominate interaction force between LNT and SPc was analyzed using ITC (TA Instruments Waters, USA). The experimental setup involved loading the cell with 2 mL of LNT aqueous solution (0.01 mmol/L), and the titration needle was charged with 250 μL of SPc aqueous solution (0.1 mmol/L). The assay was carried out at 25 °C, with a stabilization period set at 300 s and 25 titration cycles. The calorimetric data obtained from each injection were integrated to calculate the heats of interaction via NanoAnalyze™ software (USA). The ΔG was calculated using the following equation:

$$\Delta G = \Delta H - T\Delta S \quad (1)$$

The infrared spectra were investigated using FTIR (Spectrum 100 PerkinElmer, USA) to illustrate the intermolecular force between LNT and SPc. The preparatory phase involved finely grinding the test sample alongside potassium bromide (KBr, 1%), followed by desiccation under an infrared lamp to eliminate moisture. Spectroscopic measurements commenced with an initial background scan to ensure baseline accuracy, succeeded by the insertion and scanning of the sample. The spectral acquisition parameters were meticulously set to encompass a wavenumber ranging from 4000 to 500 cm^{-1}, with a wavenumber precision of 0.02 cm^{-1} and a spectral resolution of 0.4 cm^{-1}.

Particle size and morphology characterization of LNT/SPc complex

For the preparation of LNT/SPc complex, LNT standard was dissolved in ddH_2O and subsequently incubated with SPc aqueous solution at the mass ratio of 1:1. The mixture was incubated at room temperature for 15 min to facilitate the spontaneous assembly of the LNT/SPc complex. In subsequent experiments, the mass ratio of 1:1 was adopted to prepare the LNT/SPc complex, and the concentration of the LNT/SPc complex was expressed based on the concentration of LNT. The particle size distributions and zeta potentials of LNT (100 mg/L), SPc and LNT/SPc complex were measured using a Particle Sizer and Zeta Potential Analyzer (Brookhaven NanoBrook Omni, USA) at 25 °C. Each treatment included three independent samples.

The morphologies of above samples were meticulously analyzed via both SEM (JSM-6700F, Japan) and TEM (JEOL-1200, Japan). For SEM, samples (10 μL) were deposited onto silicon wafers (Beijing Zhongjing Technology Co., China), followed by air drying at 25 °C. Subsequently, a thin layer of gold was sputtered onto each sample to enhance the conductivity and image quality. The TEM preparation involved placing a droplet of each sample (10 μL) onto copper grids (Beijing Zhongjing Technology Co., China), and samples were then air dried. Each sample was further treated with 0.1% phosphotungstic acid as a negative stain to improve the contrast, followed by air drying.

TMV particle extraction and its inactivation assay by SPc

Tobacco leaves exhibiting clear infection symptoms (50 g) were pulverized in liquid nitrogen, and the resulting powder was incubated with 250 mL of Tris-HCl (pH 7.4, 0.1 mol/L). The solution underwent centrifugation at 4 °C for 10 min, and the supernatant was processed with 20% sucrose in TE buffer (pH 7.0) at 100000 g and 4 °C for 2 h. After discarding the supernatant, the sediment was resuspended in 5 mL TE buffer (pH 7.0), stored overnight at 4 °C, and subjected to further processing with 2% Triton X-100. A subsequent centrifugation step was performed under above conditions, and the sediment of TMV particles was isolated and obtained, which was then dissolved in 3 mL RNase-free ddH_2O. The concentration of TMV particles was determined using the ultraviolet spectrophotometry method. The solution of TMV particles was diluted tenfold, and its absorbance at 260 nm was measured using a UV spectrophotometer (Genesys180, USA). The TMV concentration (mg/mL) was calculated using the following formula:

$$\text{TMV concentration (mg/mL)} = (A_{260nm} \times \text{dilution ratio}) / E^{0.1\%}_{1\,cm}{}^{260nm} \quad (2)$$

The extinction coefficient ($E^{0.1\%}_{1\ cm}{}^{260\ nm}$) of TMV is 3.1.

To investigate the inactivation impacts of LNT, SPc and LNT/SPc complex, the TMV particles (50 μg/mL) were incubated with various solutions of LNT (10, 100 and 500 mg/L), SPc (0.1, 1 and 10 mg/L) and LNT/SPc complex (0.1, 1 and 10 mg/L) for 6 h, and the TEM samples were prepared as above to characterize the morphologies of treated TMV particles. Concurrently, above samples were treated with RNase A (1 μg/mL) at 37 °C for 15 min, and the total RNA was extracted from intact TMV particles using the EasyPure® Viral DNA/RNA Kit (China) and reverse transcribed using the PrimeScriptTM RT reagent Kit (Japan) to obtain the cDNA. The TMV content was quantified via qRT-PCR. Reactions were performed in triplicate using the following conditions: one cycle at 95 °C for 3 min, followed by 40 cycles at 95 °C for 5 s and 60 °C for 25 s, and a melting curve plot was constructed to confirm that no reaction produced non-specific amplification. All primers are shown in Supplementary Table 3. Additionally, the total RNA of TMV particles at concentrations of 2, 20, 200, 2000 and 20000 ng/mL was extracted, which was used to establish a standard curve for TMV particles via qRT-PCR.

Inactivation mechanism of TMV particles by SPc

The interaction of TMV particles with LNT, SPc or LNT/SPc complex was analyzed using ITC. TMV particles (0.5 mmol/L single CP protein subunit in TMV particle, 17.5 kDa) were titrated with the solution of LNT (0.1 mmol/L), SPc (0.1 mmol/L) or LNT/SPc complex (0.1 mmol/L). Additionally, the zeta potentials of TMV alone (50 mg/L) and the mixtures of TMV + LNT (TMV: 50 mg/L; LNT: 100 mg/L), TMV + SPc

(SPc: 100 mg/L) and TMV + LNT/SPc complex (LNT: 100 mg/L) were measured, and each treatment contained three independent samples. The crystal structure of TMV CP protein was downloaded from the Protein Data Bank database (ID: 6I5A). The molecular structure of LNT was obtained from the PubChem database (CID: 37723) and converted into a three-dimensional structure. The CP protein was hydrogenated and set as the receptor, and LNT was set as the ligand using AutoDock Vina V4.3 software (USA). After molecular docking, the docking result with the lowest binding energy was adopted.

The CP protein was expressed to detect the interaction of CP protein with LNT or SPc. CP protein sequence was downloaded from NCBI. Its hydrophilicity and transmembrane domains were predicted using the TOPCONS2 online platform. The His-tag and stop codon were added at the C-terminus, and the CP gene was cloned into the pKMD-SUMO (KMD bioscience Co., China) vector using the BamHI and EcoRI restriction sites. The recombinant vector was transformed into Rosetta BL21 (DE3) competent cells. The protein expression was induced by IPTG, and the expression was confirmed using the SDS polyacrylamide gel electrophoresis (SDS-PAGE). The positive BL21 strain expressing the CP protein was cultured in TB medium (1 L). The supernatant was filtered through a 220 nm membrane, and the protein was purified using the Ni-affinity chromatography (GE, USA) with the following buffers and the purified protein was analyzed using the SDS-PAGE.

Equilibration buffer: 20 mM phosphate buffer (PB) + 150 mM NaCl, pH 8.0.

Wash buffers: 20 mM PB + 150 mM NaCl + 5 mM Imidazole, pH 8.0; 20 mM PB + 150 mM NaCl + 20 mM Imidazole, pH 8.0; 20 mM PB + 150 mM NaCl + 50 mM Imidazole, pH 8.0; 20 mM PB + 150 mM NaCl + 80 mM Imidazole, pH 8.0.

Elution buffer: 20 mM PB + 150 mM NaCl + 300 mM Imidazole, pH 8.0.

The fluorescent groups were added into SPc to prepare the TPE-SPc that could be detected at 365 nm. The purified CP protein (7 μg) was incubated with LNT or TPE-SPc at the mass ratios of 1:1, 1:4 and 1:8 for 1 h, respectively. The interaction between CP protein with LNT or TPE-SPc was then assessed using Native-PAGE. Fluorescent images were captured under the $UV_{365\ nm}$ light (Amersham ImageQuant 800, Cytiva, Japan), followed by Coomassie Brilliant Blue staining to obtain protein images under visible light. The CP protein, LNT and TPE-SPc were individually employed as controls. Meanwhile, ten μL of 0.2% CP protein was spotted on positively-charged nylon membrane (Sigma, USA). The membrane was incubated in 1% BSA for 30 min, and then washed for 5 min. The above membrane was then incubated in TPE-SPc aqueous solution (1%) for 15 min[69]. Images were recorded under visible or $UV_{365\ nm}$ light (Amersham ImageQuant 800, Cytiva, Japan).

Inactivation efficacy evaluation of LNT/SPc complex against TMV particles

The inactivation efficacies of LNT/SPc complex against TMV particles in tobacco cells, seedlings and soil were individually examined in the current study. The solutions of LNT (Final concentration: 100 mg/L), SPc and LNT/SPc complex were mixed with TMV or TMV-GFP particles (Final concentration: 50 μg/mL) for 3 h to prepare the inoculation solution. The ddH_2O was employed as control.

For cell assay, each inoculation solution (2 mL) was incubated with tobacco BY2 cells and subjected to ultrasonic treatment at the intensity of 0.3 W/cm^2 for 7 min. Following 24 h of incubation at 25 °C, cellular fluorescence was observed and recorded using confocal laser scanning microscopy (Zeiss LSM 800, Germany). Total RNA was extracted from the cells using the TransZol UP Plus RNA Kit (China), and the $2^{-\Delta\Delta CT}$ method was used to quantify the gene transcript levels by qRT-PCR. The *actin* (gene ID 107831145) was used as an internal reference. Each treatment included three independent samples.

For seedling assay, above inoculation solutions (50 μL) were inoculated onto the tobacco leaves using finger rub mechanical inoculation, respectively. Each treatment contained three seedlings at six-leaf stage, which was repeated three times. Fluorescent intensity on the leaves was examined at 3 d post-inoculation, and the total RNA was extracted from the inoculated leaves using the FastPure® Universal Plant Total RNA Isolation Kit (China). The relative expression of TMV-GFP was then measured by qRT-PCR as above.

For soil assay, TMV particles (100 μg) were uniformly mixed into soil (2 g), and the 1 mL solution of LNT (1, 10 and 100 mg/L), SPc or LNT/SPc complex was added. Total RNA was extracted from the soil at 12 h post-application using the RNeasy PowerSoil Total RNA Kit (Qiagen, USA). Meanwhile, the TMV particles were mixed with soil at the mass ratios of 1, 10, 100, 1000 and 10000 ng/g (TMV: soil), and the total RNA was extracted from soil to establish a standard curve using qRT-PCR. Finally, TMV content in the soil was quantified by qRT-PCR based on above standard curve. Each treatment was repeated three times.

Contact angle and retention analysis of LNT/SPc complex

The wetting performance of LNT/SPc complex was dependent on its contact angle and retention, which were next investigated in the current study. The contact angles of LNT and LNT/SPc complex were examined using an Optical Contact Angle Meter (Date Physics Corporation OCA25, Germany). The SPc and ddH_2O were applied as controls. The 5 μL of various samples (LNT concentration: 100 mg/L) was dripped onto the glass slide, and the image of contact angle between the liquid and glass slide was collected when the droplet became stable for 10 s. The contact angle was analyzed using the ellipse fitting algorithm. The algorithm assumes that the water drop profile is part of an ellipse. Each treatment included eight independent samples.

Tobacco leaves (8 cm^2) were initially weighed to obtain the mass (M_1), and then immersed in the solutions of LNT (100 mg/L) and LNT/SPc complex for 1 min, respectively. Treated leaves were subsequently suspended in air until no droplets naturally fell off, and their weights (M_2) were recorded. The ddH_2O and SPc were employed as controls, and each treatment included eight independent leaves. The retention of each sample was calculated using the formula:

$$\text{Retention } (\text{mg/cm}^2) = (M_2 - M_1)/\text{leaf area}. \quad (3)$$

Cellular uptake of SPc-loaded fluorescent LNT

The FITC (0.1 mg) was incubated with LNT (50 mg) activated by glutaraldehyde at room temperature for 12 h, followed by dialysis using a 20000 Da dialysis bag for 24 h to remove unbound FITC, yielding FITC-LNT. FITC-LNT or FITC-LNT/SPc complex was then incubated with 2 mL of tobacco BY2 cells for 3, 6 and 12 h, followed by fixation with paraformaldehyde (4%) for 15 min. The cells were then washed three times with phosphate-buffered saline (pH 5.8) for 5 min. The ddH_2O, SPc and LNT were also used to treat the cells. The fixed cells were observed and imaged using a confocal laser scanning microscope (Zeiss LSM 800, Germany).

RNA-seq analysis for amplified plant defence induced by SPc-loaded LNT

The above results revealed the improved wetting performance and cellular uptake of LNT/SPc complex, which was beneficial for increasing the bioactivity of LNT. Thus, the plant defence induced by LNT/SPc complex was then explored in the current study. The tobacco seedlings at six-leaf stage were sprayed with the solutions of LNT (100 mg/L) and LNT/SPc complex, respectively. The whole seedlings were homogenized at 24 h after the treatment, and the total RNA was extracted using the TRNzol formulation (TIANGEN, China). Three independent seedlings were prepared for each

treatment, and each treatment was repeated three times. The transcript libraries were constructed via the Illumina Novaseq 6000 sequencing platform (Illumina, USA). Raw reads containing connectors and low-quality reads of less than Q10 were removed, and the resulting clean reads were assembled using the Trimmomatic 0.30 software (Del Lab, USA). TopHat2 (USA) was used to achieve the sequence alignment of paired-end clean reads with the reference genome (https://www.ncbi.nlm.nih.gov/datasets/genome/GCA_034376525.1/). The unigenes were annotated using BLASTX against the KEGG database. The expression level of each transcript was presented by the fragments per kilobase of transcript per million (FPKM) value. DESeq was used to analyze the DEGs between two treatments, and a fold change of ≥ 2.0 and a false-discovery rate (FDR) of <0.01 were used as the screening conditions.

Biological experiments for synergistic mechanism of SPc-loaded LNT

To verify above RNA-seq results, the expression levels of plant defence-related genes were firstly examined to illustrate the synergistic mechanism of SPc-loaded LNT. Above RNA-seq samples were reverse transcribed into cDNAs. The tobacco *actin* gene was adopted as the reference gene, and the expression levels of crucial genes such as *OLP*, *SCR2*, *CAT1*, *PER1*, *HIR1*, *WRKY53* and *PHO1* were determined using qRT-PCR.

Subsequently, the plant defence-related substances such as SA, SOD and CAT were investigated to elucidate the mechanism underlying the amplified plant defence induced by SPc-loaded LNT. The tobacco seedlings were treated with various formulations as above, and 10 g fresh leaves were ground with 20 mL aqueous ethanol (80%) at 3 d after the treatment. The ddH_2O was used as control. After centrifugation, the supernatant was concentrated to 2 mL using a rotary evaporator under vacuum (CV200, China) and then diluted to 4 mL with ddH_2O. Acetic acid was added to a final concentration of 1%, followed by 3 extractions with ethyl acetate (2 mL). The organic phase was dried under N_2 and redissolved in methanol (1 mL). Each sample was purified using a PTFE filter (220 nm) and analyzed by Ultra High-Performance Liquid Chromatograph (UHPLC, Agilent, USA) with an ACQUITY UPLC BEH C18 column (Waters Co., USA). The analytes were separated using a mobile phase composed of 0.1% acetic acid in water and methanol. The operating conditions: 10 μL injection volume per sample, 25 °C column temperature, detection wavelength of 297 nm, and flow rate of 1 mL/min. The SA standard was diluted in methanol to prepare a series dilutions of SA at the concentrations of 3.125, 6.25, 12.5, 25, 50 and 100 μg/mL, and the absorbance at 297 nm was used to construct the standard curve. The SA content was measured and calculated based on the standard curve, and each treatment contained three independent samples.

The activities of SOD and CAT were measured using the Micro Superoxide Dismutase Activity Assay Kit (Abbkine, China) and Micro Catalase Activity Assay Kit (Abbkine, China), respectively. The 0.1 g treated seedlings were homogenized in 1 mL pre-chilled lysis buffer, followed by ultrasonication (300 W, 3 s on and 7 s off) and centrifugation at 4 °C for 15 min. For SOD assay, the 20 μL supernatant was mixed with 40 μL working xanthine oxidase and 164 μL working reagent, and incubated at 37 °C for 30 min, and absorbance was measured at 450 nm using a spectrophotometer (Molecular Devices, USA). For CAT assay, the 20 μL supernatant was mixed with 100 μL assay buffer, 30 μL methanol and 20 μL diluted hydrogen peroxide solution. The mixture was incubated at room temperature for 5 min, added with 30 μL potassium hydroxide and 30 μL chromogen, and then incubated for another 10 min. Then 10 μL potassium periodate was then added, and incubated for 5 min. The absorbance at 540 nm was measured immediately. A standard curve was prepared using formaldehyde at the concentrations of 2, 5, 15, 30, 45, 60 and 75 μM. Each treatment contained three independent samples.

Control efficacy evaluation of LNT/SPc complex against TMV

Two experiments were performed independently to evaluate the preventive and curative effects of LNT/SPc complex on TMV in the laboratory. (1) Preventive effect: Solutions of LNT (100 mg/L) and LNT/SPc complex were uniformly sprayed onto tobacco seedlings at six-leaf stage, respectively. Then 50 μL TMV-GFP (20 μg/mL) was mechanically inoculated onto the third and fourth leaves by finger rubbing at 48 h after the treatment. The ddH_2O and SPc were employed as controls. Each treatment contained three seedlings, which was repeated four times. (2) Curative effect: The third and fourth leaves of seedlings were initially inoculated with 50 μL TMV-GFP (20 μg/mL) by finger rubbing, and the seedlings were sprayed with the solutions of LNT (100 mg/L) and LNT/SPc complex at 24 h post-inoculation, respectively. The third and fourth leaves were harvested and ground in liquid nitrogen at 2, 3 and 4 d post-inoculation, and the total RNA was extracted using the FastPure® Universal Plant Total RNA Isolation Kit (China) and reverse transcribed in cDNA. The relative expression of TMV-GFP was quantified by qRT-PCR as above.

Additionally, a field trial was also conducted in Shilin Yizu Autonomous County of Yunnan Province, China (24.77°N, 103.27°E, low-latitude plateau mountain monsoon climate) to assess the control efficacy of LNT/SPc complex against TMV during June 2021. Tobacco seedlings (naturally infected TMV) at root-extended period were sprayed with the solutions of LNT (40 mg/L) and LNT/SPc complex, respectively. The water and SPc were applied as controls. Each treatment contained three independent plots (Three replicates), and each plot was approximately 240 m^2. Disease grades were investigated using the following criteria at 7 and 14 d post-application. Grade 0: Whole plant disease-free; Grade 1: Heart leaf slight mosaic; Grade 3: Less than 33% leaf mosaic; Grade 5: 33% to 50% leaf mosaic; Grade 7: 51% to 67% leaf mosaic; Grade 9: More than 67% leaf mosaic. The disease index (DI) and control efficacy (CE) were calculated using the following formulas:

$$\mathrm{DI} = \left[\sum(\text{The number of plants} \times \text{disease grade value}) \div(\text{Total number of surveyed plants} \times 9)\right] \times 100 \quad (4)$$

$$\mathrm{CE}(\%) = [1 - (\text{DI of control before the treatment} \times \text{DI of treatment after the treatment}) \div(\text{DI of control after the treatment} \times \text{DI of treatment before the treatment})] \times 100 \quad (5)$$

The agronomic traits of seedlings such as plant height and the length and width of the largest leaf were finally recorded at 14 d post-application. Each treatment included 35 randomly-selected seedlings.

Safety evaluation of LNT/SPc complex toward tobacco cells and seedlings

To evaluate the safety of LNT/SPc complex in actual application, tobacco BY2 cells were incubated with SPc (100 mg/L), LNT and LNT/SPc complex at 25 °C for 12 h, respectively. After incubation, the cells were washed three times with phosphate buffer saline (PBS, pH 5.8), followed by staining with Calcein Acetoxymethyl Ester (Calcein AM) and Propidium Iodide (PI) at 37 °C for 30 min. The BY2 cells were then fixed with paraformaldehyde for observation under a confocal laser scanning microscopy (Zeiss LSM 800, Germany), and cell survival rate was subsequently recorded. Each treatment included three replicates. Additionally, tobacco seedlings at the three-leaf stage were sprayed with the solutions every 7 days for a total of 35 days, respectively. The water was employed as control. The agronomic traits of tobacco seedlings, including plant height and the length and width of the third and fourth leaves, were recorded every 7 d. Each treatment contained eighteen seedlings.

Data analysis
The statistical analysis was performed using the SPSS 26.0 software (SPSS Inc., USA). The ANOVA with Tukey HSD test or independent *t* test was used to analyze the data at the $p = 0.05$ level of significance. The descriptive statistics are shown as the mean value and standard errors of the mean.

Reporting summary
Further information on research design is available in the Nature Portfolio Reporting Summary linked to this article.

Data availability
RNA-seq data for *Nicotiana benthamiana* are available at NCBI with the accession PRJNA1154326. Figures 3a–c and 6a, b were created in BioRender. Hongyi, D. (2024) BioRender.com/t77l298. Source data are provided with this paper.

References

1. Shen, L. L. et al. Identification and purification of an antibiotic protein produced by *Pseudomonas fluorescens* strain CZ with inhibitory effect to tobacco mosaic virus. *Crop Prot,* **42**, 334–337 (2012).
2. Alonso, J. M. et al. The physics of tobacco mosaic virus and virus-based devices in biotechnology. *Trends Biotechnol,* **31**, 530–538 (2013).
3. Gao, F. L. et al. Bayesian phylodynamic analysis reveals the dispersal patterns of tobacco mosaic virus in China. *Virology* **528**, 110–117 (2019).
4. Broadbent, L. et al. Epidemiology of tomato mosaic.x. persistence of tmv-infected debris in soil and effects of soil partial sterilization. *Ann. Appl. Biol.* **55**, 471 (1965).
5. Scholthof, K. B. G. Tobacco mosaic virus: a model system for plant biology. *Annu. Rev. Phytopathol.* **42**, 13–34 (2004).
6. Gülser, C. et al. Accumulation of tobacco mosaic virus (TMV) at different depths clay and loamy sand textural soils due to tobacco waste application. *Environ. Monit. Assess.* **146**, 235–242 (2008).
7. Ellis, M. D. et al. Quantitative real-time PCR analysis of individual flue-cured tobacco seeds and seedlings reveals seed transmission of tobacco mosaic virus. *Phytopathology* **110**, 194–205 (2020).
8. Li, Y. M. et al. Seco-pregnane steroids target the subgenomic RNA of alphavirus-like RNA viruses. *Proc. Natl Acad. Sci. USA* **104**, 8083–8088 (2007).
9. Lu, Z. S. et al. Proteomic and phosphoproteomic analysis in tobacco mosaic virus-infected tobacco (*Nicotiana tabacum*). *Biomolecules* **9**, 39 (2019).
10. Wang, J. et al. Inhibitory effect of sulfated lentinan and lentinan against tobacco mosaic virus (TMV) in tobacco seedlings. *Int. J. Biol. Macromol.* **61**, 264–269 (2013).
11. Paylan, I. C. et al. Effects of different treatments on the inactivation of various seedborne viruses in some vegetables. *Ozone-Sci. Eng.* **36**, 422–426 (2014).
12. Wang, Z. W. et al. Design, synthesis, and anti-tobacco mosaic virus (tmv) activity of phenanthroindolizidines and their analogues. *J. Agric. Food Chem.* **60**, 10212–10219 (2012).
13. Liu, H. Y. et al. Characterization of anti-TMV indole alkaloid and isocoumarin derivatives from *Aspergillus versicolor* YNCA0363. *Chem. Biol. Technol. Ag.* **10**, 138 (2023).
14. Zhou, M. & Wang, W. Recent advances in synthetic chemical inducers of plant immunity. *Front. Plant Sci.* **9**, 1613 (2018).
15. El Hadrami, A. et al. Chitosan in plant protection. *Mar. Drugs* **8**, 968–987 (2010).
16. An, C. F. & Mou, Z. L. Salicylic acid and its function in plant immunity. *J. Integr. Plant Bio.* **53**, 412–428 (2011).
17. Bravo, J. et al. Effect of lipopolysaccharides from *Vibrio alginolyticus* on the Mx gene expression and virus recovery from gilthead sea bream (*Sparus aurata* L.) experimentally infected with Nodavirus. *Fish Shellfish Immun.* **34**, 383–386 (2013).
18. Kah, M. et al. Nano-enabled strategies to enhance crop nutrition and protection. *Nat. Nanotechnol.* **14**, 532–540 (2019).
19. Lowry, G. V. et al. Opportunities and challenges for nanotechnology in the agri-tech revolution. *Nat. Nanotechnol.* **14**, 517–522 (2019).
20. Rius-Rocabert, S. et al. Broad virus inactivation using inorganic micro/nano-particulate materials. *Mater. Today Bio.* **13**, 100191 (2022).
21. Esfahani, A. R. et al. Role of biofilm on virus inactivation in limestone aquifers: implications for managed aquifer recharge. *J. Environ. Health Sci.* **18**, 21–34 (2020).
22. Guo, J. F. et al. Nano delivery of chemotherapeutic icd inducers for tumor immunotherapy. *Small Methods* **7**, e2201307 (2023).
23. Ma, X. B. et al. Endogenous/exogenous stimulies inspired poly-prodrug nano-inducer switches pyroptosis path for promoting antitumor immunity. *Nano Today* **48**, 101727 (2023).
24. Gao, Y. H. et al. Facile fabrication of a fungicide and plant immune inducer co-delivery nanosystem for enhanced control efficacy against plant disease. *Chem. Eng. J.* **482**, 148817 (2024).
25. Li, J. H. et al. A facile-synthesized star polycation constructed as a highly efficient gene vector in pest management. *ACS Sustainable Chem. Eng.* **7**, 6316–6322 (2019).
26. Yan, S. et al. Self-assembled co-delivery nanoplatform for increasing the broad-spectrum susceptibility of fall armyworm toward insecticides. *J. Adv. Res.* **24**, 00044 (2024).
27. Li, M. S. et al. A gene and drug co-delivery application helps to solve the short life disadvantage of RNA drug. *Nano Today* **43**, 101452 (2022).
28. Wang, Y. X. et al. High-efficiency green management of potato late blight by a self-assembled multicomponent nano-bioprotectant. *Nat. Commun.* **14**, 5622 (2023).
29. Cai, L. et al. Preventing viral disease by ZnONPs through directly deactivating TMV and activating plant immunity in *Nicotiana benthamiana*. *Environ. Sci.: Nano* **6**, 3653–3669 (2019).
30. Liu, Y. R. et al. Star polymer-based nanodelivery system for pesticides: enhanced broad-spectrum toxicity and selective toxicity. *ACS Omega* **8**, 41595–41602 (2023).
31. Wang, X. D. et al. Field application of star polymer-delivered chitosan to amplify plant defense against potato late blight. *Chem. Eng. J.* **417**, 129327 (2021).
32. Yan, S. et al. Simple osthole/nanocarrier pesticide efficiently controls both pests and diseases fulfilling the need of green production of strawberry. *ACS Appl. Mater. Interfaces* **13**, 36350–36360 (2021).
33. Yan, S. et al. A star polycation acts as a drug nanocarrier to improve the toxicity and persistence of botanical pesticides. *ACS Sustainable Chem. Eng.* **7**, 17406–17413 (2019).
34. Su, X. F. et al. Self-assembled thiophanate-methyl/star polycation complex prevents plant cell-wall penetration and fungal carbon utilization during cotton infection by *Verticillium dahliae*. *Int. J. Biol. Macromol.* **239**, 124354 (2023).
35. Peng, H. et al. Self-assembled nanonematicide induces adverse effects on oxidative stress, succinate dehydrogenase activity, and ATP generation. *ACS Appl. Mater. Interfaces* **15**, 31173–31184 (2023).
36. Zhao, L. et al. Inhibitory effect of polysaccharide peptide (PSP) against tobacco mosaic virus (TMV). *Int. J. Biol. Macromol.* **75**, 474–478 (2015).
37. Dong, M. et al. Biotoxicity evaluation of a cationic star polymer on a predatory ladybird and cooperative pest control by polymer-delivered pesticides and ladybird. *ACS Appl. Mater. Interfaces* **14**, 6083–6092 (2022).
38. Yan, S. et al. Chronic exposure to the star polycation (SPc) nanocarrier in the larval stage adversely impairs life history traits in *Drosophila melanogaster*. *J. Nanobiotechnol.* **20**, 515 (2022).

39. Wu, S. Y. et al. Construction of a nontoxic nano-pesticide and its co-application with natural predators for perfect cooperative pest management: an innovative strategy for pesticide reduction. *Environ. Sci.:Nano* **11**, d4en00060a (2024).
40. Imani, S. M. et al. Antimicrobial nanomaterials and coatings: current mechanisms and future perspectives to control the spread of viruses including SARS-CoV-2. *ACS Nano* **14**, 12341–12369 (2020).
41. Chen, G. Y. et al. Selection and design principle of efficient antiviral nano-hybrid fiber materials for fighting pandemic viruses: a review. *Nano Today* **53**, 102001 (2023).
42. Bobrin, V. A. et al. Water-borne nanocoating for rapid inactivation of SARS-CoV-2 and other viruses. *ACS Nano* **15**, 14915–14927 (2021).
43. Ren, G. M. et al. Structural characterization and antiviral activity of lentinan from *Lentinus edodes* mycelia against infectious hematopoietic necrosis virus. *Int. J. Biol. Macromol.* **115**, 1202–1210 (2018).
44. Lanter, J. M. et al. Persistence of tomato mosaic virus in tomato debris and soil under field conditions. *Plant Dis* **66**, 552–555 (1982).
45. Yang, J. G. et al. Development of a one-step immunocapture real-time RT-PCR assay for detection of tobacco mosaic virus in soil. *Sensors* **12**, 16685–16694 (2012).
46. Sun, H. F. et al. Foliar uptake and leaf-to-root translocation of nanoplastics with different coating charge in maize plants. *J. Hazard. Mater.* **416**, 125854 (2021).
47. Brutin, D. & Starov, V. Recent advances in droplet wetting and evaporation. *Chem. Soc. Rev.* **47**, 558–585 (2018).
48. Su, Y. M. et al. Delivery, uptake, fate, and transport of engineered nanoparticles in plants: a critical review and data analysis. *Environ. Sci.: Nano* **6**, 2311–2331 (2019).
49. Jiang, Q. H. et al. Nanocarrier-loaded imidaclothiz promotes plant uptake and decreases pesticide residue. *Int. J. Mol. Sci.* **23**, 6651 (2022).
50. Yan, S. et al. Nanometerization of thiamethoxam by a cationic star polymer nanocarrier efficiently enhances the contact and plant-uptake dependent stomach toxicity against green peach aphids. *Pest Manag. Sci.* **77**, 1954–1962 (2021).
51. Ma, Z. Z. et al. Visualization of the process of a nanocarrier-mediated gene delivery: stabilization, endocytosis and endosomal escape of genes for intracellular spreading. *J. Nanobiotechnol.* **20**, 124 (2022).
52. Yang, J. et al. Construction and application of star polycation nanocarrier-based microRNA delivery system in *Arabidopsis* and maize. *J. Nanobiotechnol.* **20**, 219 (2022).
53. Choi, D. S. et al. Pepper osmotin-like protein 1 (CaOSM1) is an essential component for defense response, cell death, and oxidative burst in plants. *Planta* **238**, 1113–1124 (2013).
54. Annon, A. et al. Overexpression of a tobacco osmotin gene in carrot (*Daucus carota* L.) enhances drought tolerance. *In Vitro Cell. Dev. Pl.* **50**, 299–306 (2014).
55. Strompen, G. et al. An *as-1*-like motif controls the level of expression of the gene for the pathogenesis-related protein 1a from tobacco. *Plant Mol. Biol.* **37**, 871–883 (1998).
56. Borsics, T. & Lados, M. Dodder infection induces the expression of a pathogenesis-related gene of the family *PR-10* in alfalfa. *J. Exp. Bot.* **53**, 1831–1832 (2002).
57. Elbez, M. et al. The plant pathogenesis-related PR-10 proteins. *Acta Bot. Gallica* **149**, 415–444 (2002).
58. Grüner, R. et al. Salicylic acid and the hypersensitive response initiate distinct signal transduction pathways in tobacco that converge on the *as-1*-like element of the *PR-1a* promoter. *Eur. J. Biochem.* **270**, 4876–4886 (2003).
59. Hong, J. K. et al. Functional roles of the pepper leucine-rich repeat protein and its interactions with pathogenesis-related and hypersensitive-induced proteins in plant cell death and immunity. *Planta* **246**, 351–364 (2017).
60. Mei, Y. Z. et al. Geminivirus C4 antagonizes the *HIR1*-mediated hypersensitive response by inhibiting the *HIR1* self-interaction and promoting degradation of the protein. *New Phytol* **225**, 1311–1326 (2020).
61. Michán, S. et al. Regulation and oxidation of two large monofunctional catalases. *Free Radical Biol. Med.* **33**, 521–532 (2002).
62. Kawarazaki, T. et al. A low temperature-inducible protein AtSRC2 enhances the ROS-producing activity of NADPH oxidase AtRbohF. *Biochim. Biophys. Acta* **1833**, 2775–2780 (2013).
63. Liu, Z. Q. et al. SGT1 is required in PcINF1/SRC2-1 induced pepper defense response by interacting with SRC2-1. *Sci. Rep.* **6**, 21651 (2016).
64. Ullah, C. et al. The diversity of salicylic acid biosynthesis and defense signaling in plants: Knowledge gaps and future opportunities. *Curr. Opin. Plant Biol.* **72**, 102349 (2023).
65. Baker, A. et al. Catalase: A critical node in the regulation of cell fate. *Free Radical Bio. Med.* **199**, 56–66 (2023).
66. García-Caparrós, P. et al. Oxidative stress and antioxidant metabolism under adverse environmental conditions: a review. *Bot. Rev.* **87**, 421–466 (2021).
67. Samarah, N., Sulaiman, A., Salem, N. M. & Turina, M. Disinfection treatments eliminated tomato brown rugose fruit virus in tomato seeds. *Eur. J. Plant Pathol.* **159**, 153–162 (2021).
68. Quanrud, D. M. et al. Virus removal during simulated soil-aquifer treatment. *Water Res.* **37**, 753–762 (2003).
69. Zhou, B. C. et al. An AIE star polymer with enhanced co-delivery of durg and gene for synergistic pest control. *Chin. J. Chem.* **41**, 2671–2678 (2023).

Acknowledgements

This work was supported by the Foundation of Yunnan Tobacco Company (grant number: 2021530000241018) to S.Y.; The National Natural Science Foundation of China (grant numbers: 32372631; 32072497) to S.Y.; The Pinduoduo-China Agricultural University Research Fund (grant number: PC2023B02018) to S.Y. We thank Prof. Tao Zhou for providing the TMV and Prof. Jing Zhang for providing the tobacco BY2 cells.

Author contributions

S.Y., J.S., Y.X., and Q.J. designed the project and interpreted the data. Q.J. performed most of the experiments. B.Z. performed ITC experiments. S.Y., Q.J., J.S., and J.Z. analyzed the data. Z.W., D.N., and H.L. provided tobacco resources. M.Y. provided nanomaterial resources. S.Y. and Q.J. wrote the manuscript. All authors edited the manuscript.

Competing interests

The authors declare no competing interests.

Additional information

Supplementary information The online version contains supplementary material available at https://doi.org/10.1038/s41467-024-52851-z.

Correspondence and requests for materials should be addressed to Jie Shen or Shuo Yan.

Peer review information *Nature Communications* thanks Xianchao Sun and the other, anonymous, reviewer(s) for their contribution to the peer review of this work. A peer review file is available.